

Deep level transient spectroscopy characterization without the Arrhenius plot

Cite as: Rev. Sci. Instrum. 92, 023902 (2021); doi: 10.1063/5.0039555

Submitted: 4 December 2020 • Accepted: 9 January 2021 •

Published Online: 1 February 2021



View Online



Export Citation



CrossMark

Jian V. Li^{a)} 

AFFILIATIONS

Department of Aeronautics and Astronautics, National Cheng Kung University, 1 University Road, Tainan 70101, Taiwan

^{a)}Author to whom correspondence should be addressed: jianvli@mail.ncku.edu.tw

ABSTRACT

Defect characterization by deep level transient spectroscopy (DLTS) requires the extraction of two key quantities of the carrier emission rate from the defects—activation energy (E_a) and pre-exponential factor (v_0)—the latter is related to the carrier capture cross section. This task, ubiquitous to thermally activated processes besides defect–carrier interaction, is traditionally accomplished by constructing an Arrhenius plot with DLTS peak locations and fitting it with a line. We present a transformation method based on the Arrhenius equation that extracts E_a and v_0 *without constructing or line-fitting the Arrhenius plot* and bypasses peak identification. This method is developed on the basis of the fundamental temperature-rate duality relationship and extracts E_a and v_0 by matching the curvatures the Arrhenius-transformed spectra of the iso-thermal and iso-rate DLTS scans in the 2D temperature-rate plane. The extraction can be conducted with data in a small temperature range and is, therefore, capable of unambiguously resolving E_a and v_0 at any temperature point and their temperature dependence, if any.

Published under license by AIP Publishing. <https://doi.org/10.1063/5.0039555>

I. INTRODUCTION

Deep level transient spectroscopy (DLTS) was invented by Lang¹ in 1974. Since then, it has been widely used as the workhorse measurement and instrumentation for detecting electrically active defects² in semiconductor materials³ and characterizing their properties: type, concentrations, energetic locations, and carrier capture cross sections. In its most common implementation,¹ a DLTS apparatus probes the capacitance transient during the emission stage of carriers from certain defect, which in the preceding capturing stage has been filled with the said carriers. The polarity and magnitude of this capacitance transient signal can be used to determine the defect type and density, respectively. The exponentially decaying time dependence of the capacitance transient allows the rate-window treatment of DLTS electronics (e.g., via boxcar averaging¹ or a lock-in amplifier⁴) to measure the emission rate of carriers, which is described by²

$$\nu = v_0 \exp(-E_a/k_B T), \quad (1)$$

where ν is the emission rate of carriers from a defect located at an energetic distance of E_a away from one of the carrier conduction band edges, v_0 is the attempt-to-escape frequency, which also

contains information regarding the carrier capture cross section,² k_B is Boltzmann's constant, and T is the temperature. The symbol E_a stands for activation energy, implying that Shockley–Read–Hall emission of carriers from a defect is a thermal activation process^{5,6} and that Eq. (1) is essentially the Arrhenius equation.⁷ Indeed, the application of the DLTS technique has been extended from defects to other thermally activated phenomena in semiconductors, such as carrier transport near a quantum well.⁶

The accurate measurement of the activation energy E_a and the attempt-to-escape frequency v_0 by DLTS is, therefore, critical to understanding the electrical defects and other thermally activated phenomena in semiconductors. To date, DLTS characterization of E_a and v_0 has been almost exclusively following the standard procedure of the Arrhenius plot line-fitting (APL) method:¹ (i) The rate-window treated DLTS signal is recorded as a function of temperature. (ii) In a DLTS spectrum, one observes a defect-induced peak and identifies the peak temperature, which varies with the rate window. Note that the polarity of the peak may be either positive or negative (i.e., valley), indicating minority and majority carrier trapping defects, respectively. (iii) One then plots the semi-logarithmic plot of rate-window vs inverse peak temperature, i.e., an Arrhenius plot of $\ln(\nu_{peak})$ vs T^{-1}_{peak} . (iv) Finally, a line fitting according to

Eq. (1) is performed to the Arrhenius plot data to extract E_a and v_0 from the slope and intercept with the ordinate, respectively.

The classical Arrhenius plot line-fitting method, although deceptively simple, usually requires several (5–7 at a minimum) data points in practice to yield a high-quality extraction. To ensure a sufficient number of peak data points and the rate/temperature range of observation for a reliable line fitting, one is motivated to scan a wide range of rate-windows and temperatures, which demands more sophisticated DLTS electronics and cryogenic temperature control apparatus. On the other hand, if the same defect signature is observed over a wide range of rate-temperature, then there is the possibility that the Arrhenius plot data points do not strictly conform to a straight line, i.e., the Arrhenius plot is *curved*. This indicates a non-Arrhenius process in which E_a and v_0 vary with temperature,⁸ as opposed to a strictly Arrhenius process where E_a and v_0 are invariant over temperature. The APL method has rather limited power against such non-Arrhenius processes because it is impossible to extract two temperature dependent functions of $E_a(T)$ and $v_0(T)$ independent of only one set of data v_{peak} (T_{peak}).

It, thus, appears that, despite being very mature, there is still room for improvement and innovation for the classical Arrhenius plot line-fitting method. Resolving the temperature dependence of E_a and v_0 of non-Arrhenius processes is desirable because it may unlock a wealth of information⁹ hitherto hidden in the Arrhenius plot. In this work, we demonstrate a method to extract E_a and v_0 from DLTS scanning spectra *without using the Arrhenius plot*. This method is developed on the basis of the fundamental temperature-rate duality relationship.¹⁰ We employ transformations based on the Arrhenius equation to project experimental iso-rate and iso-thermal DLTS scans taken from the 2D temperature-rate plane to other parameter spaces. E_a and v_0 are extracted by matching the curvatures of the projected DLTS scanning spectra.

II. EXPERIMENTAL

We used a SULA Technologies system to collect the DLTS data. The core piece of the SULA DLTS system is a Boonton capacitance meter 7200 that uses a capacitance bridge to capture the capacitance transient at 1 MHz modulation frequency. A GaAs solar cell sample was used to demonstrate the DLTS method developed in this work, although any other Schottky or PN junction with suitable defect would serve the purpose. The device is an asymmetrical n⁺-p junction with 1 × 1 cm² device area grown by metal-organic chemical vapor deposition under less-than-optimized conditions and known to contain deep defects similar to those reported in Ref. 11. The carrier concentration on the p-side was determined to be $2 \times 10^{15} \text{ cm}^{-3}$ by capacitance-voltage measurements conducted at 1 kHz and room temperature. The GaAs sample was subject to the same electrical conditions during the DLTS measurements: the quiescent reverse bias was set at −0.6 V, the filling pulse had a pulse height of 1.0 V, and the width of the filling pulse was 10 ms. DLTS spectra were collected at 12 rate window settings—0.02 ms, 0.05 ms, 0.1 ms, 0.2 ms, 0.5 ms, 1 ms, 2 ms, 5 ms, 10 ms, 20 ms, 50 ms, and 100 ms.

One calibrated silicon-diode type temperature sensor (Lakeshore DT-670-SD) was embedded inside an oxygen-free beryllium copper sample stage attached to the cold head of a

closed-cycle He-cooled cryostat (Janis model M-22). Two 25-Ω cartridge heaters were inserted between the cold head of the cryostat and the sample stage to provide the means of heating the latter. The temperature of the sample stage was stabilized at any setting temperature between 12 K and 450 K, to within 0.01 K precision, through a proportional-integral-derivative control algorithm optimized for the above thermal system. A second calibrated silicon-diode type temperature sensor (Lakeshore DT-670-SD) was mechanically clamped directly on top of the sample to ensure the best thermal contact to the sample. The sample temperature was scanned downward at a rate of 10 K/min in this work.

We used all the twelve rate-window setting allowed by the SULA DLTS system to acquire raw DLTS spectra shown in Fig. 1. Due to the hardware configuration of the DLTS system, the 12 DLTS spectra were collected in three separate temperature scans, each collecting DLTS spectra for four rate-window settings. Two peaks are clearly identifiable each indicative of the presence of one defect. The negative peak is due to the majority-carrier trapping defect. The positive peak is due to the minority-carrier trapping defect. The emission rate v corresponding to the peak temperature observed in the DLTS spectra is related¹ to the rate window according to $v = (4.3 \times \text{rate window})^{-1}$. The DLTS spectra taken at different rate-windows show some artifacts of baseline drift and amplification inhomogeneity due to the hardware electronics, which do not affect the extraction of peak positions in the APL method but will affect the Arrhenius transformation based method developed in this work and need to be removed.

According to the conventional practice, an Arrhenius plot of the emission rates vs the peak temperatures observed in DLTS spectra can be constructed, as shown in Fig. 2 (symbols). As expected, the data resemble a line and can be fitted by a line (Fig. 2, line) to extract the defect activation energy from its slope of and the attempt-to-escape frequency from its intercept with the ordinate. The extracted activation energies are $0.698 \pm 0.005 \text{ eV}$ and $0.965 \pm 0.029 \text{ eV}$ for the majority and minority carrier trapping defects, respectively. The corresponding attempt-to-escape frequencies expressed in natural logarithmic, i.e., $\ln(v_0)$, are $24.0 \pm 0.2 \text{ ms}^{-1}$ and $26.9 \pm 0.9 \text{ ms}^{-1}$,

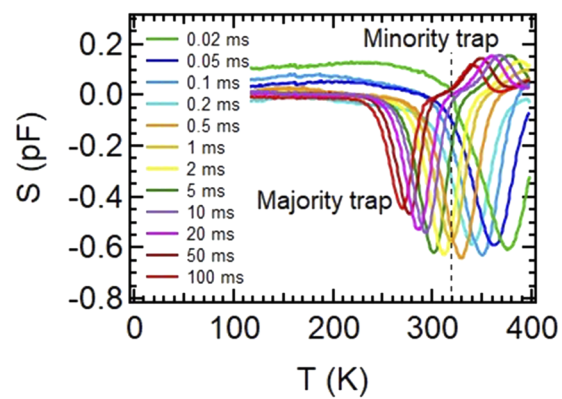


FIG. 1. The raw iso-rate deep level transient spectroscopy spectra measured at various window settings exhibit two peaks indicative of the presence of the two defects. The negative peak is due to the majority-carrier trapping defect. The positive peak is due to the minority-carrier trapping defect.

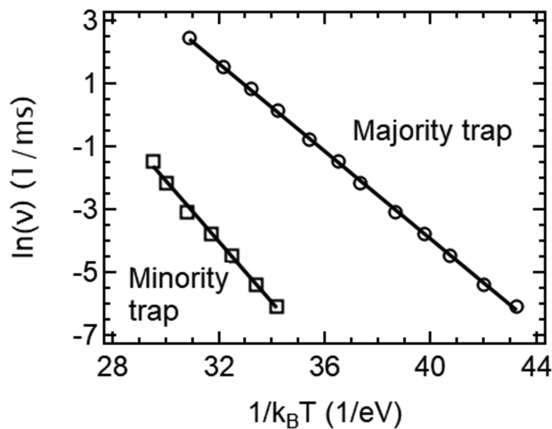


FIG. 2. The Arrhenius plot of the raw iso-rate deep level transient spectroscopy data peaks observed in Fig. 1 (symbols) and the line fitting (line) are used to extract the defect activation energies of 0.698 ± 0.005 eV and 0.965 ± 0.029 eV for the majority and minority carrier trapping defects, respectively. The corresponding attempt-to-escape frequencies expressed in natural logarithmic, i.e., $\ln(v_0)$, are 24.0 ± 0.2 ms $^{-1}$ and 26.9 ± 0.9 ms $^{-1}$, respectively.

respectively. The Arrhenius plot of the majority carrier trapping defect comprises of 12 data points, collected from 269 K to 377 K, which contributes to the good quality of the line fitting yielding a high linear correlation coefficient of 0.9998. In contrast, the Arrhenius plot of the minority carrier trapping defect comprises of only seven data points collected from 340 K to 395 K; hence, its line fitting quality is relatively poor yielding a relatively low linear correlation coefficient of 0.9957. The fitting quality is also manifested by the relatively significant amount of scattering of data around the fitting line and the much larger one-standard-deviation error for the minority carrier trapping defect. This comparison demonstrates that a sufficient number of data points in the Arrhenius plot, taken over a sufficient wide range of rate/temperature, are required to achieve reliable high-quality fitting and extraction of E_a and v_0 .

A critical inspection of the classic Arrhenius plot line-fitting method reveals that the DLTS electronics measures the raw DLTS signal, $S(T)$, to extract the peak positions T of $S(T)$ at various rate settings of v . The information, thus, retrieved for the Arrhenius plot analysis, v_{peak} (T_{peak}), is necessarily one-dimensional. If the one-dimensional data v_{peak} (T_{peak}) are deemed to be of linear nature, then only two extractable parameters are produced through a line fitting, E_a and concomitantly v_0 , for the entire scanning range of rate-temperature. The above analysis shows that the APL method cannot unambiguously measure E_a and v_0 and their temperature dependence. This is an inherent deficiency of the APL method when facing the possibility of temperature dependent E_a and v_0 .

III. RESULTS

The development of a new method to extract E_a and v_0 without an Arrhenius plot is found on the rate-temperature duality, first realized by Agarwal *et al.*¹⁰ in DLTS and later applied to admittance spectroscopy.¹² Note that the two parameters of v and T in Eq. (1)

are independently controllable in a DLTS experiment. Because v and T are related by Eq. (1) in the same thermal activation process defined by the same E_a and v_0 , a scan in v -space corresponds to an equivalent scan in T -space, and vice versa. Consequently, scanning either v or T while keeping the other constant leads to DLTS responses that contain identical information.

We define the iso-rate scan as a DLTS scan that varies the temperature T while keeping the rate v constant, as shown in Fig. 1. An iso-thermal scan then refers to a scan that varies with the rate v , while keeping the temperature T constant. During the first decades following the conception of DLTS, the iso-rate scan had been the default choice of instrument due to hardware and software resource constrictions, which is now largely relaxed. Figure 3 shows an iso-thermal scan carried out at 318.4 K using data reconstructed from those presented in Fig. 1. The iso-thermal scan also exhibits a peak that is the signature of the same majority carrier trapping defect seen in the iso-rate scan.

Of course, one can repeat the iso-thermal scan at various temperatures and record the peak positions of the defect signature, which are then used to construct an Arrhenius plot to extract E_a and v_0 according to the same procedure as iso-rate scans (Fig. 2). The above reconstruction of the iso-thermal scan and ensuing Arrhenius plot analysis do not deviate from the original iso-rate scan based method in principle.¹³ The extractions of E_a and v_0 from iso-thermal scans agree with those using the iso-rate scans, and no revelation of new physics is expected. That is to say, if either of the two scans—iso-rate or iso-thermal—is conducted to extract E_a and v_0 via the Arrhenius plot line fitting, one is still limited by the same shortcomings mentioned above because both analyses only retrieved information from the simple peak positions of the DLTS spectra.

Next, we break through the limit of the classical APL method by simultaneously exploiting the iso-thermal and iso-rate DLTS

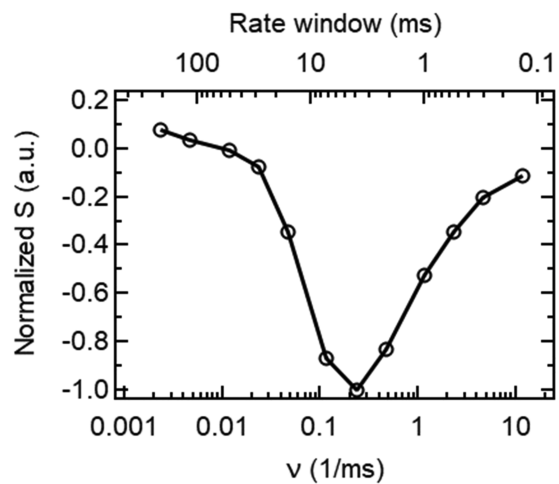


FIG. 3. The raw iso-rate deep level transient spectroscopy spectra measured at various window settings are used to reconstruct an iso-thermal scan, which also exhibit a peak indicative of the presence of one majority-carrier trapping defect (the negative peak). Only the iso-thermal scan at one temperature of 318.4 K (indicated by the dashed lines in Fig. 1) is shown.

scans and retrieving information from the *curvatures* of both spectra. Essentially, the new method takes full use of the entire *two-dimensional* rate-temperature space to maximize the information retrievable, thus overcoming the fundamental one-dimensional limitation of the APL method. From the Arrhenius equation of Eq. (1), we further derive the following two Arrhenius transformations that use v_0 as a free-tuning parameter, and T and v as experimentally controlled variables:

$$E_{a,T} = k_B T \ln(v_0/v_{fix}), \quad (2)$$

$$E_{a,v} = k_B T_{fix} \ln(v_0/v). \quad (3)$$

We use Eqs. (2) and (3) as the $v-E_a$ and $T-E_a$ transformations to project the experimental iso-thermal and iso-rate scans, $S(v)$ and $S(T)$, onto the activation energy space as virtual scans $S(E_{a,v})$ and $S(E_{a,T})$, respectively. The two experimental scans $S(v)$ and $S(T)$ probe the activation behavior of the same thermal activation process. Therefore, the two virtual scans $S(E_{a,v})$ and $S(E_{a,T})$ should agree with each other in the energy space, if and only if the best fit v_0 used in the $T-E_a$ and $v-E_a$ transformations is true to the thermal activation process physically responsible to both scans—this is the basis for the extraction of v_0 . Once v_0 is determined according to the above fitting procedure, E_a is computed by using Eq. (1) since E_a and v_0 are related by Eq. (1) at (T_{fix}, v_{fix}) . E_a can also be taken directly from the common peak position shared by $S(E_{a,T})$ and $S(E_{a,v})$. If desired, the above procedure can be repeated at different temperatures to yield the temperature dependent $E_a(T)$ and $v_0(T)$. We call the above method used to extract E_a and v_0 the Arrhenius transformation and matching (ATM) method.

We now apply the ATM method in our case study of electronic transitions due to defects in GaAs. The raw DLTS spectra in Fig. 1 are normalized to the maximum DLTS negative peak amplitude (corresponding to 0.5 ms rate window) to remove electronics-induced artifacts mentioned earlier. This step is of course optional and depends on the DLTS electronics. Figure 4 shows the contour

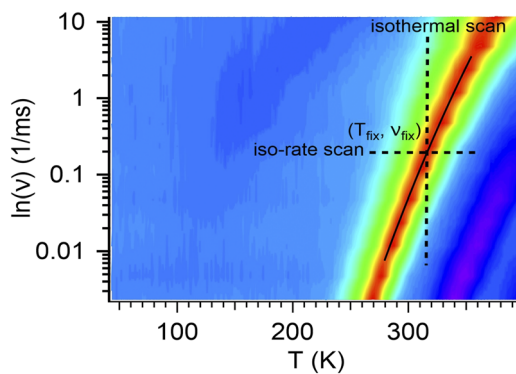


FIG. 4. The contour plot of the normalized deep level transient spectroscopy signal S is displayed in the temperature-rate plane. Warmer colors correspond to more negative values of S . The solid black line indicates the locus of peak points (T, v) used to construct the Arrhenius plot. The iso-thermal and iso-rate scans at any (T_{fix}, v_{fix}) point (one example shown in dashed lines) may be used to extract the E_a and v_0 through the ATM method using suitable transformation parameters.

plot of the normalized DLTS signal S displayed in the $T-v$ plane. The classic APL method exploits only the first moment (i.e., the locus of peak positions in the $T-v$ space indicated by the thick solid line in Fig. 4) of $S(T, v)$ to produce the Arrhenius plot data v_{peak} (T_{peak}) for line fitting. The information, thus, retrieved for the Arrhenius plot analysis is one dimensional in nature.

In contrast, the ATM method exploits the second moment of S (e.g., the curvature of the surface) in the $T-v$ space by simultaneously matching the iso-thermal and iso-rate scans at a (T, v) point (example shown by thin dashed lines near T_{fix} and v_{fix} in Fig. 4) to extract E_a and v_0 . An example of this variation of the ATM method, i.e., with T and v projected onto the activation energy space, is illustrated in Fig. 5. We transformed the experimental iso-thermal scan $S(v)$ taken at 318.4 K (Fig. 3) using the $T-E_a$ transformation in Eq. (2) to obtain the virtual scan $S(E_{a,T})$ in the activation energy space (Fig. 5, dashed line and symbols). We transformed the experimental iso-rate scan $S(v)$ taken at 1 ms rate window, which corresponds to $\ln(v_{fix}) = -1.45 \text{ ms}^{-1}$, using the $v-E_a$ transformation in Eq. (3) to obtain the virtual scan $S(E_{a,v})$ in the activation energy space (Fig. 5, solid line). That $S(E_{a,v})$ agrees well with $S(E_{a,T})$ in a range $\sim 20 \text{ K}$ nearby 318.4 K attests the good quality of extraction. The attempt-to-escape frequency value used in both Eqs. (2) and (3) was $\ln(v_0) = 24 \text{ ms}^{-1}$, from which the activation energy $E_a = 0.698 \text{ eV}$ was calculated according to Eq. (1) at $T_{fix} = 318.4 \text{ K}$ and $\ln(v_{fix}) = -1.45 \text{ ms}^{-1}$. E_a can also be taken directly from the common peak position shared by $S(E_{a,T})$ and $S(E_{a,v})$.

Equating the right-hand side of Eqs. (2) and (3), we arrive at

$$T = T_{fix}^* (\ln v_0 - \ln v) / (\ln v_0 - \ln v_{fix}), \quad (4)$$

which we call the $v-T$ transformation. Consider the two independent scans obtained through separate experiments (similar to those in Figs. 1 and 3): (i) the iso-rate scan $S(T)$ as T is scanned with v fixed at v_{fix} and (ii) the iso-thermal scan $S(v)$ as v is scanned with T fixed at T_{fix} . For an experimentally obtained iso-thermal scan $S(v)$ in v -space, we use the $v-T$ transformation in Eq. (4) to transform from

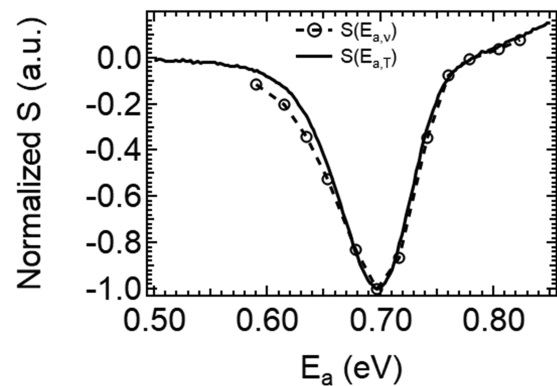


FIG. 5. The iso-thermal scan $S(v)$ (dashed line and symbols) and iso-rate scan $S(T)$ (solid line) taken at $T_{fix} = 318.4 \text{ K}$ and $\ln(v_{fix}) = -1.45 \text{ ms}^{-1}$ (corresponding to a rate window of 1 ms), respectively, are projected onto the activation energy space by Eqs. (2) and (3) using the best fit value of $\ln(v_0) = 24 \text{ ms}^{-1}$ to produce good matching between the virtual scans of $S(E_{a,v})$ and $S(E_{a,T})$. The E_a value of 0.698 eV is calculated from Eq. (1) using $\ln(v_0) = 24 \text{ ms}^{-1}$ at (T_{fix}, v_{fix}) .

v to T and obtain a corresponding virtual scan $S(T_v)$ in T -space. Note that only one of the two parameters of E_a and v_0 is free tuning in Eq. (4) because they both satisfy Eq. (1) at $T = T_{fix}$ and $v = v_{fix}$. In the following procedure, we use E_a as the free tuning parameter. The two experimental scans $S(v)$ and $S(T)$ probe the activation behavior of the same thermal activation process. Therefore, the virtual scan $S(T_v)$ transformed from $S(v)$ and the experimental iso-rate scan $S(T)$ should agree with each other, if and only if the $v-T$ transformation uses the E_a value true to the thermal activation process physically responsible to both scans—this is the basis for the extraction of E_a . Once E_a is determined according to the above fitting procedure, v_0 is computed by Eq. (1) since E_a and v_0 are related by Eq. (1) at (T_{fix}, v_{fix}) . An example of this variation of the ATM method, i.e., with the $v-T$ transformation, is illustrated in Fig. 6 using the same $S(v)$ and $S(T)$ data as in Fig. 5.

As is often the case, the DLTS electronics and software may be designed to work preferentially with either the iso-rate scan or the iso-thermal scan, not both. One can extend the ATM method with projection to the activation energy space to apply to only one type of scans, either iso-rate or iso-thermal. This operation is demonstrated in Fig. 7. The four $S(T)$ scans with the fastest rate-window settings are not included because they contain excessive hardware-related offset and drift issues (Fig. 1). The other eight iso-rate $S(T)$ scans are projected to the activation energy space via Eq. (2) using the same v_0 . The eight virtual $S(E_{a,T})$ spectra overlap with each other with good agreement. This attests to the fact that the DLTS transfer function,¹⁴ which relates the fundamental electronic structure (i.e., density of states) of defects to their DLTS signal, remains largely invariant across the particular range of rate window settings used. In practice, one can conduct the $T-E_a$ transformation to project the iso-rate scans taken at various rate windows to energy space and require all the $S(E_{a,T})$ spectra to agree with each other, thus achieving an effective method to extract v_0 also without the Arrhenius plot. E_a can then simply be taken directly from the common peak position

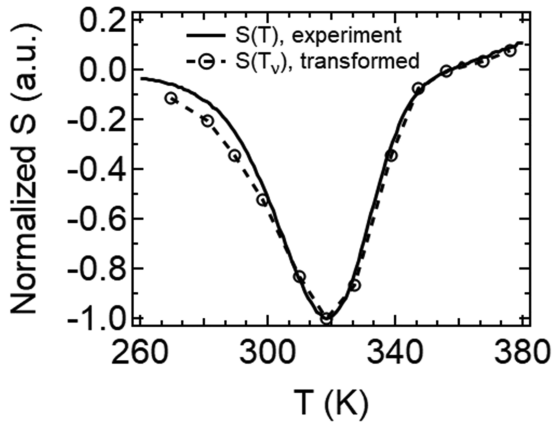


FIG. 6. The virtual iso-rate scan of $S(T_v)$ (dashed line and symbols) is obtained via the $v-T$ transformation [Eq. (4)] of the experimental iso-thermal scan $S(v)$ (solid line) at $T_{fix} = 318.4$ K. When a best fit transformation parameter $\ln(v_0) = 24 \text{ ms}^{-1}$ is used, $S(T_v)$ matches a separate experimental iso-rate scan $S(T)$ taken at $\ln(v_{fix}) = -1.45 \text{ ms}^{-1}$ (corresponding to a rate window of 1 ms). The E_a value of 0.698 eV is calculated from Eq. (1) using $\ln(v_0) = 24 \text{ ms}^{-1}$ at (T_{fix}, v_{fix}) .

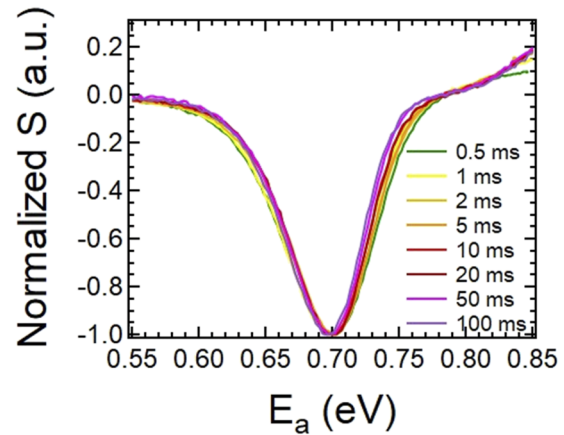


FIG. 7. The iso-rate scans taken at eight different rate-window settings are projected onto the activation energy space by Eq. (2) to produce the virtual scans $S(E_{a,T})$. When a suitable transformation parameter $\ln(v_0) = 24 \text{ ms}^{-1}$ is used, all eight virtual scans overlap with each other indicating good agreement and extraction quality. The E_a value of 0.698 eV is simply read from the common peak shared by all eight transformed scans, or calculated from Eq. (1) using $\ln(v_0) = 24 \text{ ms}^{-1}$ at (T_{fix}, v_{fix}) .

shared by the $S(E_{a,T})$ spectra. Walter *et al.* demonstrated¹⁵ similar collapsing results using admittance spectroscopy, but they did not proceed to propose a method to extract E_a and v_0 .

IV. DISCUSSION

We note that the underlying assumption of the APL method, yielding a single value of E_a and v_0 , is for both parameters to be invariant over the entire $T-v$ space scanned in the experiment. In contrast, when the data fitting of the ATM method is confined to a small range near T_{fix} and v_{fix} (e.g., $\sim T_{fix} \pm 10$ K in Fig. 5), then the activation energy project method extracts E_a and v_0 that are *local* to that (T_{fix}, v_{fix}) point. Since the two scans are performed on physically independent variables, i.e., mutually orthogonal, they do not have measurement related correlations. The ATM extraction of E_a at $T = T_{fix}$ is then accomplished by matching the curvatures of $S(T)$ to $S(T_v)$ without other arbitrary constraints such as invariance over temperature. The ATM method, thus, takes advantage of the two-dimensional data from the $S(T, v)$ surface acquired via a matrix scan of S in the $T-v$ plane. The physical information contained in $S(T, v)$, a 2D array of size $N \times M$ ($N > 2$ and $M > 2$ are the number of T and v data points, respectively), is more than sufficient for solving two independent size- N 1D arrays $E_a(T)$ and $v_0(T)$.

In Arrhenius processes, the temperature dependence of E_a is negligible such that both the APL and ATM methods yield similar results. As explained above, the ATM method may reveal details of the temperature dependent behavior of E_a and v_0 not possible by the classic APL methods. Although the defects in the GaAs sample used in this work do not show strong temperature dependence of E_a and v_0 , evidences are ample in other physical and material systems.⁹ An admittance spectroscopy based defect study in copper indium gallium selenide¹² demonstrated strong temperature

dependence of E_a and v_0 , indicative of strong non-Arrhenius nature of the defect activation, which manifest the Meyer–Neldel rule¹⁶ by varying temperature in a single sample only, in contrast to previous studies that require either multiple samples or additional physical quantities besides temperature.

We point out that other ATM variations of scanning and transformation are possible by exploiting the E_a – v_0 symmetry in Eq. (1). Similar to T – E_a and v – E_a transformations, we define the T – v_0 transformation as

$$v_0 = v_{fix} \exp(E_a/k_B T), \quad (5)$$

and the v – v_0 transformation as

$$v_0 = v \exp(E_a/k_B T_{fix}). \quad (6)$$

In these two transformations, T and v are also experimentally controlled variables, but E_a is the free tuning variable. One then uses E_a as the fitting parameter to project the experimental iso-thermal and iso-rate scans onto the attempt-to-escape frequency space. Matching these projected iso-thermal and iso-rate scans in the attempt-to-escape frequency space determine the best choice of E_a , from which v_0 is calculated according to Eq. (1) at (T_{fix}, v_{fix}) . In case only one kind (iso-rate or iso-thermal) of scan is available, one of the corresponding transformations [Eqs. (5) or (6)] can be used to project multiple scans of the particular kind to the attempt-to-escape frequency space and extract E_a and v_0 when all transformed scans collapse on top of each other.

One can also devise the T – v transformation from equating the right-hand side of Eqs. (5) and (6), which is the reverse of the v – T transformation in Eq. (4),

$$v = v_{fix}^* \exp(E_a/k_B T - E_a/k_B T_{fix}). \quad (7)$$

This transformation projects the experimental iso-rate scan $S(T)$ conducted at v_{fix} onto the rate space and produce a virtual iso-thermal scan $S(v_T)$, which are then matched to the experimental iso-thermal scan $S(v)$ conducted at T_{fix} to extract E_a and v_0 . This variation may prove advantageous in more recent DLTS electronics where digitization and signal processing enable the collection of experimental iso-thermal scanning with a wide range of rate windows at fixed temperatures.

The APL method depends on resolving the peaks in the DLTS spectra $S(T)$, which is affected by the correlation functions of the DLTS electronics, to extract the peak positions used by line-fitting of the Arrhenius plot to extract E_a and v_0 . The ATM method is not immune to the same broadening effects but uses a single operation of transforming and matching the shapes of iso-rate and iso-thermal DLTS scans to extract E_a and v_0 . In this regard, the ATM method is akin to the DLTS spectral fitting methods.¹⁴ The “matching” of the two experimental curves requires merely their numerical agreement, which is less demanding than curve fitting of $S(T)$ because neither the form of DLTS spectral $S(T)$ nor its peak position need to be explicitly known. Because the ATM method extracts E_a and v_0 by matching the iso-rate and iso-thermal scans, it does not extract the trap concentration n_t or its depth profile, which is conventionally derived from the peak amplitude of $S(T)$ via visual reading or curve fitting. In this aspect, the ATM method offers neither advantage nor loss of functionality compared to the APL method. By the

same token, the sensitivity of DLTS detection and extraction, which is often coupled with its spectral selectivity (resolution) discussed earlier, is not expected to be adversely affected by the ATM method.

V. CONCLUSIONS

In conclusion, we have devised a DLTS characterization method to extract the activation energy E_a and pre-exponential factor v_0 of the carrier emission process from the defects *without using the Arrhenius plot*. This ATM method is developed on the basis of fundamental temperature-rate duality relationship and uses the Arrhenius equation to transform temperature and rate to each other, or both to the activation energy and attempt-to-escape spaces. Extraction of E_a and v_0 is accomplished by matching the transformed DLTS scans with each other or to a separate experimental scan. The extraction can be done at any temperature point and, therefore, is able to unambiguously solve E_a , v_0 , and their temperature dependence.

ACKNOWLEDGMENTS

The author thanks Dr. S. Kurtz for providing the GaAs sample and Dr. S. W. Johnston for teaching him the DLTS technique. This research was in part supported by Ministry of Science and Technology, Taiwan, through Grant No. MOST-107-2218-E-006-022-MY3. The author also acknowledges the support from the Window on Science Program of U.S. Air-Force Office Science and Research.

DATA AVAILABILITY

The data that support the findings of this study are available from the corresponding author upon reasonable request.

REFERENCES

- ¹D. V. Lang, *J. Appl. Phys.* **45**, 3023 (1974).
- ²P. Blood and J. W. Orton, *The Electrical Characterization of Semiconductors: Majority Carriers and Electron States* (Academic Press, London, 1992).
- ³*Capacitance Spectroscopy of Semiconductors*, edited by J. V. Li and G. Ferrari (Pan Stanford Publishing, Singapore, 2018).
- ⁴A. Elhami Khorasani, D. K. Schroder, and T. L. Alford, *IEEE Trans. Electron Devices* **61**, 3282 (2014).
- ⁵C. T. Sah, *Fundamentals of Solid-State Electronics* (World Press, Singapore, 1990).
- ⁶D. V. Lang, “Measurement of band offsets by space charge spectroscopy,” in *Heterojunction Band Discontinuities: Physics and Device Applications*, edited by F. Capasso and G. Margaritondo (Elsevier, 1987).
- ⁷S. Arrhenius, *Z. Phys. Chem.* **4**, 226 (1889).
- ⁸C. H. Henry and D. V. Lang, *Phys. Rev. B* **15**, 989 (1977).
- ⁹D. Wickramaratne, C. E. Dreyer, B. Monserrat, J.-X. Shen, J. L. Lyons, A. Alkauskas, and C. G. Van de Walle, *Appl. Phys. Lett.* **113**, 192106 (2018).
- ¹⁰S. Agarwal, Y. N. Mohapatra, and V. A. Singh, *J. Appl. Phys.* **77**, 3155 (1995).
- ¹¹S. W. Johnston, R. S. Crandall, and A. Yelon, *Appl. Phys. Lett.* **83**, 908 (2003).
- ¹²J. V. Li, S. W. Johnston, Y. Yan, and D. H. Levi, *Rev. Sci. Instrum.* **81**, 033910 (2010).
- ¹³J. V. Li and D. H. Levi, *J. Appl. Phys.* **109**, 083701 (2011).
- ¹⁴A. A. Istratov, H. Hieslmair, C. Flink, and E. R. Weber, *Rev. Sci. Instrum.* **69**, 244 (1998).
- ¹⁵T. Walter, R. Herberholz, C. Müller, and H. W. Schock, *J. Appl. Phys.* **80**, 4411 (1996).
- ¹⁶A. Yelon, B. Movaghari, and R. S. Crandall, *Rep. Prog. Phys.* **69**, 1145 (2006).